AD-A118 346 AEROSPACE CORP EL SEGUNDO CA CHEMISTRY AND PHYSICS LAB F/G 11/6
AN ANALYTICAL MODEL FOR RF INDUCTIVE GLOW DISCHARGE COLUMNS IN --ETC(U)
JUL 82 H U ECKERT F04701-81-C-0082
UNCLASSIFIED TR-0082(2472-06)-1 SD-TR-82-47 NL

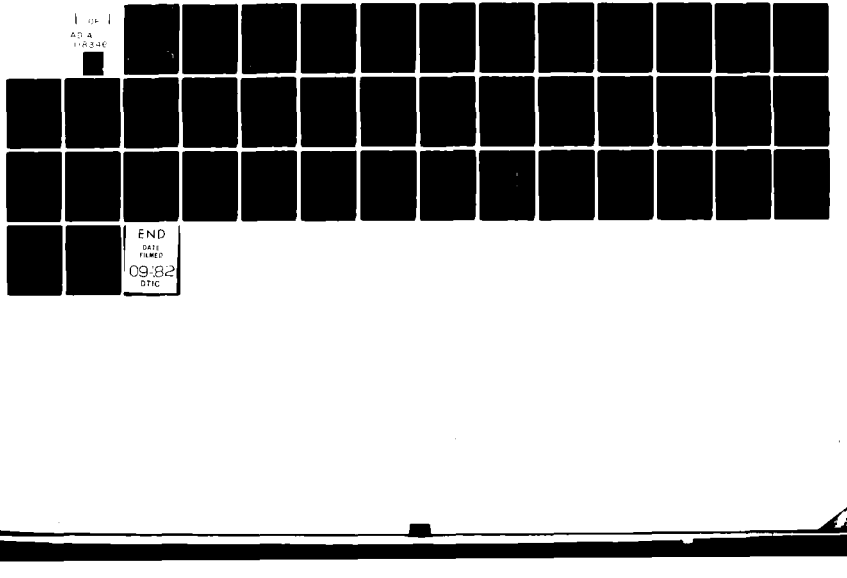

REPORT SD-TR-82-47

An Analytical Model for rf Inductive Glow Discharge Columns in Metal-Gas Mixtures and Application to the Rb-Xe System

HANS U. ECKERT, Consultant
Chemistry and Physics Laboratory
Laboratory Operations
The Aerospace Corporation
El Segundo, Calif. 90245

12 July 1982

Prepared for
SPACE DIVISION
AIR FORCE SYSTEMS COMMAND
Los Angeles Air Force Station
P.O. Box 92960, Worldway Postal Center
Los Angeles, Calif. 90009

This report was submitted by The Aerospace Corporation, El Segundo, CA 90245, under Contract No. F04701-81-C-0082 with the Space Division, Deputy for Technology, P.O. Box 92960, Worldway Postal Center, Los Angeles, CA 90009. It was reviewed and approved for The Aerospace Corporation by S. Feuerstein, Director, Chemistry and Physics Laboratory. Lt Efren V. Fornoles, SD/YLXT, was the project officer for Technology.

This report has been reviewed by the Public Affairs Office (PAS) and is releasable to the National Technical Information Service (NTIS). At NTIS, it will be available to the general public, including foreign nations.

This technical report has been reviewed and is approved for publication. Publication of this report does not constitute Air Force approval of the report's findings or conclusions. It is published only for the exchange and stimulation of ideas.

Efren V. Fornoles

Efren V. Fornoles, 1st Lt, USAF
Project Officer

Jimmie H. Butler

Jimmie H. Butler, Colonel, USAF
Director of Space Systems Technology

FOR THE COMMANDER

Norman W. Lee

Norman W. Lee, Jr., Col, USAF
Deputy for Technology

UNCLASSIFIED

SECURITY CLASSIFICATION OF THIS PAGE (When Data Entered)

REPORT DOCUMENTATION PAGE		READ INSTRUCTIONS BEFORE COMPLETING FORM
1. REPORT NUMBER SD-TR-82-47	2. GOVT ACCESSION NO. AD-A118346	3. RECIPIENT'S CATALOG NUMBER
4. TITLE (and Subtitle) AN ANALYTICAL MODEL FOR RF INDUCTIVE GLOW DISCHARGE COLUMNS IN METAL-GAS MIXTURES AND APPLICATION TO THE Rb-Xe SYSTEM		5. TYPE OF REPORT & PERIOD COVERED 6. PERFORMING ORG. REPORT NUMBER TR-0082(2472-06)-1
7. AUTHOR(s) Hans U. Eckert		8. CONTRACT OR GRANT NUMBER(s) F04701-81-C-0082
9. PERFORMING ORGANIZATION NAME AND ADDRESS The Aerospace Corporation El Segundo, California 90245		10. PROGRAM ELEMENT, PROJECT, TASK AREA & WORK UNIT NUMBERS
11. CONTROLLING OFFICE NAME AND ADDRESS Space Division Air Force Systems Command Los Angeles, California 90009		12. REPORT DATE 12 July 1982 13. NUMBER OF PAGES 39
14. MONITORING AGENCY NAME & ADDRESS(if different from Controlling Office)		15. SECURITY CLASS. (of this report) Unclassified 15a. DECLASSIFICATION/DOWNGRADING SCHEDULE

16. DISTRIBUTION STATEMENT (of this Report)

Approved for public release; distribution unlimited.

17. DISTRIBUTION STATEMENT (of the abstract entered in Block 20, if different from Report)

18. SUPPLEMENTARY NOTES

19. KEY WORDS (Continue on reverse side if necessary and identify by block number)

Alkali Vapor, Alkali Vapor Noble Gas Mixture, Electroless Discharge Lamp, Glow Discharge Column, Rubidium-Xenon Spectral Lamp

20. ABSTRACT (Continue on reverse side if necessary and identify by block number)

The electron balance equation is solved for a glow discharge column excited by rf induction in a metal vapor - noble gas mixture where the metal atoms are ionized in a single step and ionization of the gas is negligible. The accumulation of metal atoms near the wall is accounted for by postulating for their radial distribution n(r), a power law with positive exponent. Under this condition, the profile for the electron density $n_e(r)$ can be expressed by zero order Bessel functions containing a profile parameter q that is related to the exponent in the atomic distribution n(r). q is evaluated as a function of rf

DD FORM 1473 (FACSIMILE)

UNCLASSIFIED

SECURITY CLASSIFICATION OF THIS PAGE (When Data Entered)

19. KEY WORDS (Continued)

20. ABSTRACT (Continued)

power input and electron temperature T_e for a fixed column radius R = 0.4 cm by solving the electron energy balance equation for $T_e = f(r)$. The profiles n(r) and $n_e(r)$ are interrelated by the condition that in a steady state their slopes at r = R must be proportional to the ambipolar and atomic diffusion coefficients, respectively. This and the common boundary condition $n_e(R) = 0$ provide additional relationships that permit presentation of q as a function of the two control variables: power input per unit column length, P/L, and mean concentration of metal atoms and positive ions, n_t, (determined by the vapor pressure). The equations are applied to a Rb-Xe mixture with p(Xe) = 2 Torr. The ionization rate coefficient for Rb is derived approximately from measurements of ionization cross sections assuming a Maxwellian distribution f for the electron energies. Calculations of $n_e(r)$ and n(r), carried out for two values of P/L, indicate a tendency for the profiles to assume a rectangular shape with increasing P/L, which agrees qualitatively with observations in Cs - Ar dc columns. The values of T_e associated with the calculated cases are higher than observed in Rb-Xe rf-excited lamps and suggest that multistep ionization may not be negligible.

CONTENTS

FIGURES

I. INTRODUCTION

Dc and ac discharges in mixtures of a metal vapor with a noble gas have found wide applications in space illumination and their properties have been studied extensively by experiment and theory [1-12]. More recently, low power versions of such discharges have been used for optical pumping in various devices including atomic frequency standards [13-19]. In this case the metal is usually rubidium, and it has been found preferable to excite the discharge electrodelessly by rf induction [15, 16]. Neither the gaseous electronic properties of this metal nor the details of this excitation method are well known, so that the understanding of this kind of discharge is in a rudimentary state and its development has been carried out largely on empirical grounds. On the other hand, there are high demands on stability, efficiency and useful life for these discharge lamps, notably in space-borne equipment, which necessitate a thorough understanding of the ongoing processes. In this paper a first step toward such understanding is made through establishment of a simple mathematical model that correlates some internal parameters of the discharge with external parameters and yields closed form expressions for the radial distributions of electrons and metal atoms. The metal vapor complicates the situation compared to that in a simple gas discharge by its tendency to segregate from the buffer gas. This is due to the fact that the metal atoms, having a considerably lower ionization potential than the gas atoms, provide most of the ionization, although their average concentration is generally lower by orders of magnitude. The metal ions travel with the fast electrons in ambipolar diffusion to the wall where they recombine and return as atoms into the discharge volume. Since this back diffusion occurs at a slower rate, the metal atom concentration builds up near the wall and may exceed here their average concentration several times. It is of importance to know the metal atom concentration directly at the wall, since a small fraction is retained there and lost from the discharge process through some

physical or chemical process. As long as the retained atoms can be replaced by vaporization from a pool, their number in the volume remains constant and the radiation output steady. Once, however, this supply is exhausted, the output declines and the lamp fails. Being able to correlate the lamp life with the wall atom concentration would help in a quantitative description of the interaction process. Since this concentration is difficult, if not impossible to measure, one depends on calculations, for which the model will be useful.

Knowledge of temperature and particle distributions is also important for understanding the radiation characteristics of the lamp, notably, the degree of self absorption experienced by the resonance radiation before leaving the plasma.

The operational stability of the lamp also depends on the distribution of particles and electric fields. It is well known that a low-pressure rf induction discharge at small power inputs usually starts in a capacitive mode; upon an increase of power it abruptly switches to the inductive mode and vice versa. The presence of two species with different ionization potentials enhances the possibility for mode switching.

So it is expected that the model developed in the following, which to the author's knowledge represents the first closed-form treatment for this kind of discharge, can help on a variety of problems.

II. ANALYSIS

a) Radial Distributions of Electrons and Metal Atoms

We consider an axially uniform plasma column of radius R that contains free electrons, metal atoms and singly charged ions at concentrations n_e, n and n_i, respectively, which are functions of the radial coordinate r. Noble gas atoms which are present at concentrations higher by several orders of magnitude do not participate in the ionization, but determine the diffusion rates of atoms and charged particles. As mentioned, there is a counterflow between electrons and ions moving to the wall and recombined atoms returning into the plasma. Since any new electron-ion pair generated means the loss of an atom, the divergences of the two flows are oppositely equal

$$\nu_i n_e = \nabla \Gamma_e = -\nabla \Gamma \qquad (1),(2)$$

where ν_i is the ionization frequency of an average electron and Γ_e and Γ are the densities of electron and atom fluxes, respectively. Since both fluxes start with zero at their respective origins r = 0 and r = R, we also have

$$\Gamma_e = -\Gamma \qquad (3)$$

For the one dimensional column

$$\Gamma_e = -D_a \frac{dn_e}{dr}, \qquad (4)$$

and,

$$\Gamma = -D \frac{dn}{dr}. \qquad (5)$$

Combining Eqs. (4) and (5) with Eq. (3) yields

$$\frac{dn_e}{dr} = -\frac{D}{D_a} \frac{dn}{dr} \qquad (6)$$

a result obtained already by Waszink and Polman [4]. D and D_a, the atomic and ambipolar diffusion coefficients, which are essentially functions of the gas temperature T and the electron temperature T_e,

are considered to be independent of radial position. With Eq. (4) we can write the electron balance equation (1)

$$\frac{d^2 n_e}{dr^2} + \frac{1}{r} \frac{dn_e}{dr} + \frac{\nu_i}{Da} n_e = 0 \tag{7}$$

ν_i is proportional to the local value of n and can be expressed by

$$\nu_i = k_{gi} n \tag{8}$$

where k_{gi} is the ionization rate coefficient of ground state atoms. It is a function of T_e. The distribution of n is assumed to follow the power law

$$n = n_R \left(\frac{r}{R}\right)^{2q} \tag{9}$$

where n_R is the value of n at $r = R$ and $q > 0$. Using Eq. (9) and setting $r/R \equiv \rho$ we can write Eq. (7)

$$\frac{d^2 n_e}{d\rho^2} + \frac{1}{\rho} \frac{dn_e}{d\rho} + R^2 \frac{\nu_{iR}}{D_a} \rho^{2q} n_e = 0 \tag{10}$$

where $\nu_{iR} \equiv k_{gi} n_R$

The solution of Eq. (10) can be written

$$n_e = n_{e_o} J_o \left[\frac{R}{q+1} \left(\frac{\nu_{iR}}{D_a}\right)^{1/2} \rho^{q+1}\right] \tag{11}$$

where n_{e_o} is the value of n_e at $r = 0$ and J_o is the Bessel function of zero order. Setting at the wall, $\rho = 1$, $n_e = 0$ which is admissible, if the electron mean free path $\ell << R$, we obtain $J_o(\lambda) = 0$ where

$$\lambda = 2.405 = \frac{R}{q+1} \left(\frac{\nu_{iR}}{D_a}\right)^{1/2} \tag{12}$$

Besides at the axis, where it is automatically satisfied, condition (6) will be satisfied at the wall. This yields by differentiation of Eqs. (9) and (11) for $\rho = 1$

$$2q\, n_R = n_{e_o}\, (q+1)\, \frac{D_a}{D}\, \lambda\, J_1(\lambda) \tag{13}$$

where J_1 is the first-order Bessel function. Replacing n_R by the average atom density $\bar{n}$, which through Eq. (9) is related to n_R by

$$n_R = \bar{n}\,(q+1) \tag{14}$$

Eq. (13) reduces to

$$2q\bar{n} = n_{e_o}\, \frac{D_a}{D}\, \lambda\, J_1(\lambda) \tag{15}$$

Likewise the peak electron density n_{e_o} can be replaced by the mean value

$$\bar{n}_e = 2\, n_{e_o}\, I_1(q) \tag{16}$$

where

$$I_1(q) \equiv \int_0^1 J_o\left(\lambda \rho^{q+1}\right) \rho\, d\rho \tag{17}$$

is plotted in Fig. 1.

Because of charge neutrality $\bar{n}_e = \bar{n}_i$,

we have

$$\bar{n}_e + \bar{n} = \bar{n}_t \tag{18}$$

where $\bar{n}_t$ is the total average concentration of metal atoms and ions. It is given by

$$\bar{n}_t = \frac{p_v(T_{min})}{kT} \tag{19}$$

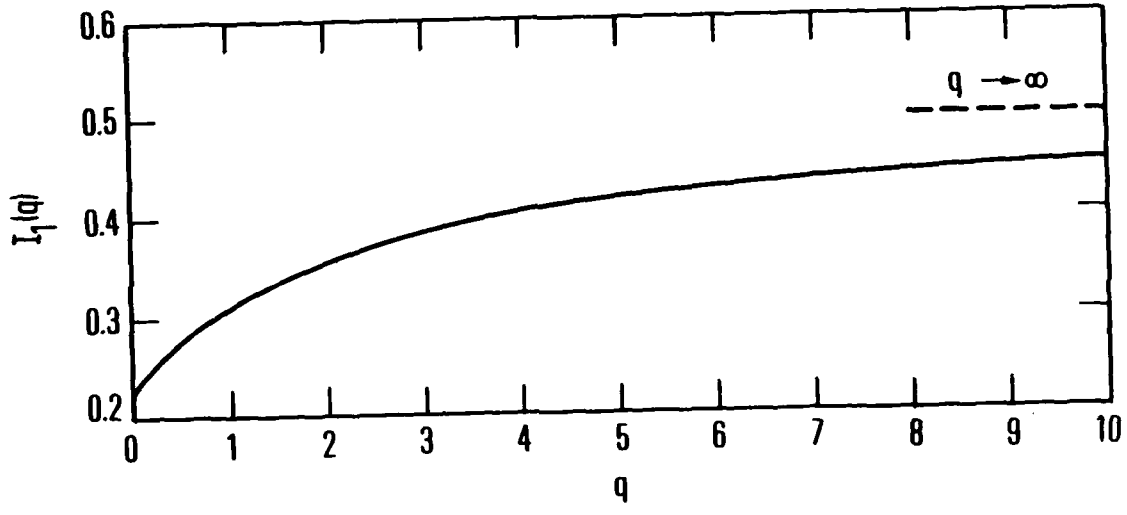

Figure 1. The Function $I_1(q) \equiv \int_0^1 J_0(\lambda\rho^{q+1})\rho\, d\rho$

where $p_v(T_{min})$ is the metal vapor pressure at the point of minimum temperature on the inside wall surface and k is the Boltzmann constant. $\bar{n}_t$ is considered to be one of the input variables. The other independent variable is the power dissipated in the discharge column, for which an expression will be derived in the next section.

b) Dissipation of rf Power

The input of power P into the discharge column occurs inductively by an rf magnetic field of angular frequency ω. The power dissipated per unit of column length L follows from the common expression

$$\frac{P}{L} = 2\pi R^2 \int_0^1 \sigma E^2 \rho \, d\rho \tag{20}$$

where the electrical conductivity σ and the induced electric field E are both functions of ρ. In an rf field the real part of σ is related to n_e, ω and the electron-neutral collision frequency ν_c by

$$\sigma = \frac{n_e e^2 \nu_c}{m_e (\nu_c^2 + \omega^2)} \tag{21}$$

where e and m_e are the electronic charge and mass, respectively.

The variation of E can be expressed to good approximation [20] by

$$E = E_R \rho^P \tag{22}$$

where E_R is the value of E at the boundary.

The exponent p is a function of the ratio R/δ, where δ is the skin depth. For $R/\delta \leq 1$, $p \approx 1$; for $R/\delta > 1$, $p \longrightarrow R/\delta$. δ is defined by

$$\delta = \left(\frac{2}{\bar{\sigma}\, \omega\, \mu_o} \right)^{1/2} \tag{23}$$

where μ_o is the magnetic permeability of the vacuum.

Although E has a strongly nonuniform distribution across the column, it has been found by several experimenters [21-23] that the electron temperature T_e in low-pressure induction discharges with noble gases is little affected by this nonuniformity and can, to a good approximation, be taken as constant. There may be two different reasons for this result. In the first place it is apparently a consequence of the high thermal conductivity of the electron component which averages out nonuniformities in T_e. Secondly, there is usually a capacitive electric field from the inductor coil present in the discharge which, unlike the induced field, does not vanish at the axis. Although its contribution to the total power input is small, it has a marked effect on the equalization of T_e, as was noticed by Turban [24] for a discharge in hydrogen.

We thus have a justification for combining the electron density profile Eq. (11), obtained for uniform T_e, with the nonuniform field distribution Eq. (22) into the expression for the power input Eq. (20). Making also use of Eqs. (11), (12) and (21), we obtain

$$\frac{P}{L} = \frac{2\pi R^2 n_{e_o} e^2 \nu_c E_R^{\,2}}{m_e (\nu_c^{\,2} + \omega^2)} \int_0^1 J_o (\lambda \rho^{q+1})\, \rho^{2p+1}\, d\rho \tag{24}$$

In many practical cases Eq. (24) can be simplified. Since the vapor pressure of the metal is usually in the milli-Torr region and by several orders of magnitude lower than that of the buffer gas, the effective degree of ionization is small, even if the vapor is fully ionized. For values of $\bar{n}_e$ in the order of $10^{12} - 10^{14}\,cm^{-3}$, $\nu_c \sim 10^9 - 10^{10}\,sec^{-1}$, $\omega \sim 10^8 - 10^9\,sec$

and $R \sim 1$ cm, it follows from what is said above and Eqs. (21) and (23) that $R/\delta \sim 1$, so that $p \sim 1$. Also, one can in Eqs. (21) and (24) generally disregard ω^2 against ν_c^2. In the following these simplifications have been used. The integral of Eq. (24) has been evaluated for $p = 1$ and is plotted in Fig. 2. It will be referred to as $I_2(q)$.

Electrons, which are the primary recipients of the rf power, transmit it partly to the heavy particles through elastic and inelastic collisions, and partly to the wall through ambipolar diffusion with positive ions by releasing their kinetic energy and the heat of recombination.

We thus have

$$\frac{P}{L} = \left(\frac{P}{L}\right)_{gas} + \left(\frac{P}{L}\right)_{wall} \tag{25}$$

Disregarding the much less frequent inelastic collisions and considering, besides T_e, also the gas temperature T as constant, we may write

$$\left(\frac{P}{L}\right)_{gas} = 2\pi R^2 \frac{3}{2} \zeta k (T_e - T) \nu_c \int_0^1 n_e \rho \, d\rho \tag{26}$$

where ζ is the fraction of its energy an average electron loses per elastic collision and is approximately $= 2m_e/M$, (M = mass of heavy particle). Using the distribution $n_e(\rho)$ of Eq. (11) as well as the identity (17), Eq. (25) can be written

$$\left(\frac{P}{L}\right)_{gas} = 3\pi R^2 \zeta k (T_e - T) n_{e_o} I_1(q) \tag{27}$$

The portion of power delivered directly to the wall by the electrons is

$$\left(\frac{P}{L}\right)_{wall} = -2\pi D_a \left(\frac{dn_e}{d\rho}\right)_R (eV_i + \frac{5}{2} kT_e) \tag{28}$$

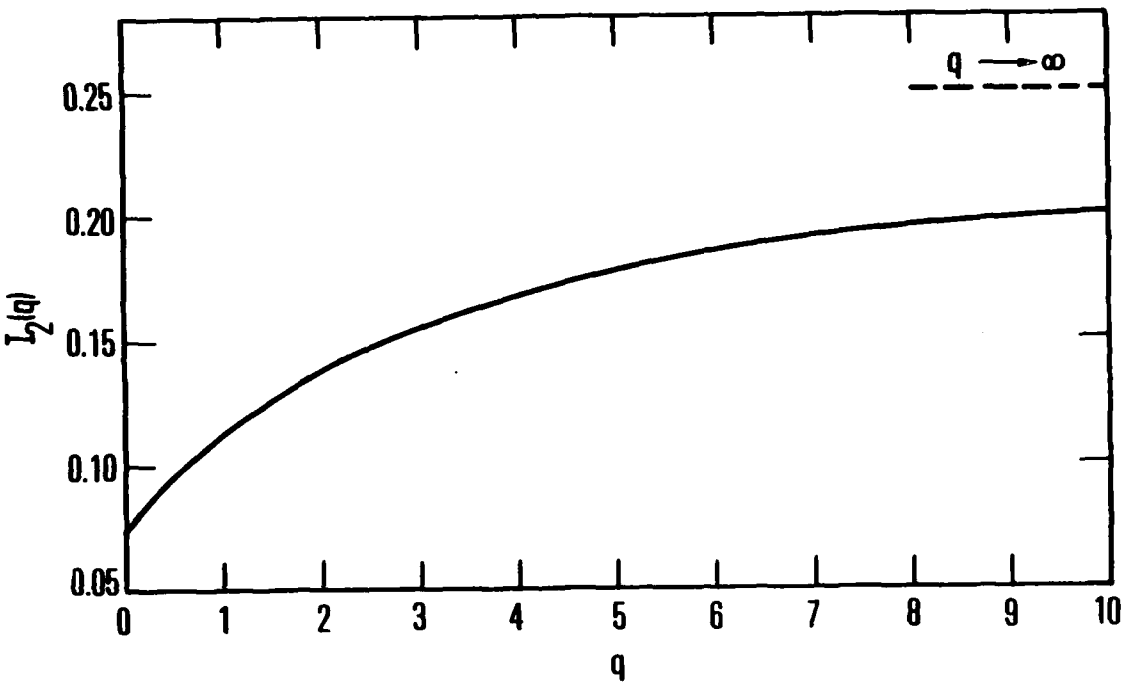

Figure 2. The Function $I_2(q) \equiv {}_0\int^1 J_0(\lambda\rho^{q+1})\rho^3 d\rho$

or when $(dn_e/d\rho)_R$ is eliminated by the differentiated Eq. (11) and Eq. (12)

$$\left(\frac{P}{L}\right)_{wall} = 2\pi D_a n_{e_o} \left(e V_i + \frac{5}{2} k T_e\right) (q+1)\lambda J_1(\lambda) \tag{29}$$

It is seen from Eqs. (24), (27) and (29) that the total power as well as the gas and wall portions are proportional to n_{e_o}. Thus, when these equations are substituted into Eq. (24), n_{e_o} cancels out. This permits us to evaluate the induced electric field at the wall, E_R, as a function of T_e and q for particular metal-gas mixtures and known values of R and T.

Carrying out the substitution with the simplified form of Eq. (24) and with

$$\int_0^1 J_o (\lambda \rho^{q+1}) \rho^3 \, d\rho \equiv I_2(q) \tag{30}$$

yields

$$E_R^2 = \frac{m_e \nu_c}{e^2 I_2(q)} \left[\frac{3}{2} \zeta \nu_c k (T_e - T) I_1(q) + \frac{D_a}{R^2} \left(eV_i + \frac{5}{2} k T_e\right) (q+1) \lambda J_1(\lambda) \right] \tag{31}$$

c) Solution of System of Equations

Once E_R has been determined from Eq. (31), the further procedure is as follows:

E_R is fed back into Eq. (24) to obtain the ratio $n_{e_o} L/P$ as a function of T_e and q. To eliminate n_{eo}, we combine Eqs. (12), (14) and (15), remembering that $\nu_{iR} = K_{gi} n_R$, obtain

$$n_{e_o} = \frac{2q}{J_1(\lambda)} \frac{(q+1}{R^2} \frac{D(T)}{k_{gi}(T_e)} \tag{32}$$

Eq. (32) in combination with Eq. (24) thus enables us to plot P/L as a function of q and T_e. For a given value of P/L we then obtain a multitude of couples q_i, T_i that all are possible solutions. The particular couple that applies to a specific case is the one that also satisfies Eq. (18) which, with the use of Eqs. (12), (14), (16) and (32), can be written as

$$\bar{n}_t = \frac{\lambda(q+1)}{R^2 k_{gi}(T_e)} \left[\lambda D_a(T_e) + \frac{4q I_1(q)\, D(T)}{J_1(\lambda)} \right] \tag{33}$$

Once a unique value for q has been determined, one has the complete information for calculating the distributions of n and n_e from Eqs. (9) and (11), respectively, with aid of Eqs. (12) and (14).

In the next chapter application of the method to a particular metal-gas mixture and specific input conditions will be illustrated.

III. APPLICATION TO Rb-Xe SYSTEM

a) Collision Frequency and Diffusion Coefficients

The analysis developed in the preceding chapter has been applied to an rf inductive glow discharge in Xe seeded with Rb which, as mentioned, is of interest as a radiation source for atomic frequency standards and other optically pumped devices. For the particular case investigated, the Xe fill pressure is 2 Torr which, according to Ref[21], corresponds to an electron collision frequency $\nu_c = 9.1 \times 10^9$ sec.$^{-1}$. A gas temperature T = 400 K has been assumed. The diffusion coefficient of Rb atoms in Xe has been calculated from the well-known expression

$$D = \frac{\ell \bar{v}}{3} \tag{34}$$

where according to Mc Daniel [25] the mean free path of the Rb atoms is given by

$$\ell = \left\{ 2^{1/2} \pi n d^2 + \pi n' \left[1/2 (d + d')\right]^2 \left(1 + \frac{M}{M'}\right)^{1/2} \right\}^{-1} \tag{35}$$

d means the atomic diameter and primed symbols refer to Xe. Since n is several orders of magnitude lower than n', the first term in Eq. (35) may be disregarded. With d = 0.504 nm one obtains

$$\ell = 1.53 \times 10^{-3} \text{ cm} \tag{36}$$

The mean velocity of the Rb atoms follows from

$$\bar{v} = \left(\frac{8kT}{\pi M}\right)^{1/2} = 3.14 \times 10^4 \text{ cm sec}^{-1} \tag{37}$$

Inserting (36) and (37) into Eq. (34) yields

$$D = 16.0 \text{ cm}^2 \text{ sec}^{-1} \tag{38}$$

The ambipolar diffusion coefficient, defined by

$$D_a = \frac{\mu_e D_i + \mu_i D_e}{\mu_e + \mu_i}, \tag{39}$$

can be approximately calculated from

$$D_a \approx \frac{\mu_i D_e}{\mu_e} \tag{40}$$

A value for μ_i, the mobility of Rb ions in Xe, has been obtained from Loeb [26]. At T = 293K and p = 760 Torr the value is 1.12 $cm^2 x$ $(V\ sec)^{-1}$. Correcting for the effects of p and T on particle density, we obtain for the present case

$$\mu_i = 581\ cm^2\ (V\ sec)^{-1} \tag{41}$$

Since

$$\frac{D_e}{\mu_e} = kT_e \tag{42}$$

we obtain from (40) with (41) and (42)

$$D_a = 5.01 \times 10^{-2} T_e \tag{43}$$

b) Ionization Rate Coefficient of Rb Atoms

The dependence of the ionization rate coefficient k_{gi} upon the electron temperature has been derived from measurements of the ionization cross section Q_{gi} with low-energy electron beams.*

*Attempts have also been made to derive values for k_{gi} more directly from the measurements by Solov'ev et al. [30-34] in Rb glow discharges. These values are by up to six orders of magnitude below those from the above method and, in the present application, would involve unrealistically high values of T_e. Since the authors claim to be able to separate single-step from multiple-step ionization coefficients, their work will be restudied for the development of a three-level discharge model.

The qualitative measurements by Tate and Smith [27] which have been calibrated by Brink [28] and are for Rb in good agreement with the more recent data by Mc Farland and Kinney [29], were used.

k_{gi} is obtained by averaging Q_{gi} over the range of electron velocities

$$k_{gi} = \overline{Q_{gi}(\epsilon)\, v_e(\epsilon)} \tag{44}$$

where v_e is the velocity of an individual electron and ϵ is its kinetic energy. The averaging is carried out by integration over the electron energies from ionization $\epsilon_i = eV_i$ to infinity

$$k_{gi} = \int_{\epsilon_i}^{\infty} Q_{gi}(\epsilon)\, v_e(\epsilon)\, f_e(\epsilon)\, d\epsilon \tag{45}$$

where f_e is the electron energy distribution function. Q_{gi} is approximated by the slope of the experimental curve at the origin $\epsilon = \epsilon_i$

$$Q_{gi} = \left(\frac{\Delta Q_{gi}}{\Delta \epsilon}\right)_{\epsilon_i} (\epsilon - \epsilon_i) \tag{46}$$

as it is common practice (see f.i. von Engel [35]). v_e is given by

$$v_e = \left(\frac{2}{m_e}\right)^{1/2} \epsilon^{1/2} \tag{47}$$

The electron energy distribution is assumed to be Maxwellian which according to earlier calculations by Margenau [36] represents a closer approximation to actual conditions in rf discharges than in dc discharges.

In this case

$$f_e \, d\epsilon = \frac{2}{\pi^{1/2}} \left(\frac{\epsilon}{\epsilon_m}\right)^{1/2} e^{-\frac{\epsilon}{\epsilon_m}} \, d\left(\frac{\epsilon}{\epsilon_m}\right) \tag{48}$$

where $\epsilon_m = k T_e$

Introducing Eqs. (46) to (48) into Eq. (45) then yields

$$k_{gi} = \left(\frac{2}{m_e}\right)^{1/2} \frac{2}{\pi^{1/2}} \left(\frac{\Delta Q_{gi}}{\Delta \epsilon}\right)_{\epsilon_i} \int_{\epsilon_i}^{\infty} \epsilon^{1/2} \left(\epsilon - \epsilon_i\right) \left(\frac{\epsilon}{\epsilon_m}\right)^{1/2} e^{-\left(\frac{\epsilon}{\epsilon_m}\right)} d\left(\frac{\epsilon}{\epsilon_m}\right)$$

or

$$k_{gi} = \left(\frac{8}{\pi m_e}\right)^{1/2} \left(\frac{\Delta Q_{gi}}{\Delta \epsilon}\right)_{\epsilon_i} \epsilon_m^{\frac{3}{2}} \int_{X_i}^{\infty} X(X - X_i) \, e^{-X} \, dX \tag{50}$$

where $X \equiv \frac{\epsilon}{\epsilon_m}$ and $X_i \equiv \frac{\epsilon_i}{\epsilon_m}$.

The integral in Eq. (50) yields

$$(X_i + 2) \, e^{-X_i} \tag{51}$$

From the experimental data [27 - 29] we have obtained

$$\left(\frac{\Delta Q_{gi}}{\Delta \epsilon}\right)_{\epsilon_t} = 3.76 \times 10^{-16} \ \frac{cm^2}{eV} \tag{52}$$

with the numerical values, (51), and

$X_i = \frac{e V_i}{k T_e}$, we obtain from Eq. (50)

$$k_{gi} = 2.015 \times 10^{-14} T_e^{3/2} \left(3 \frac{e V_i}{k T_e} - 2 \right) e^{- \frac{e V_i}{k T_e}} \qquad (53)$$

Eq. (53) has been evaluated with V_i (Rb) = 4.18 V and is plotted in Fig. 3. Also shown is the ratio k_{gi}/D_a.

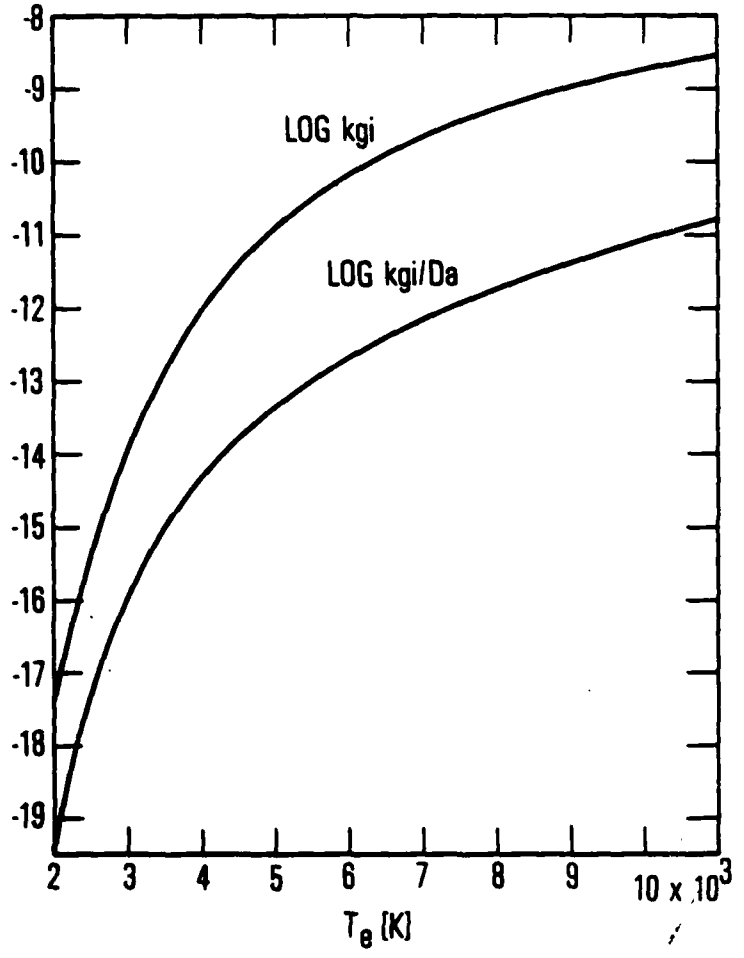

Figure 3. Ionization Rate Coefficient k_{gi} for Rb Ground-State Atoms and the Ratio k_{gi}/D_a for Rb-Xe Mixture as Functions of Electron Temperature

IV. RESULTS

a) Data for Profile Parameters

For calculating the radial distributions of n and n_e from Eqs. (9) and (11) for a given radius R, we have to determine, in addition to the common profile parameter q, the values of n_R and n_{e_o}. This is facilitated by the charted material of this section for a particular radius R = 0.4 cm. The quantities E_R and T_e, which enter into the relationships between dependent and independent variables and characterize the discharge conditions, will also be presented graphically.

In Fig. 4 is shown the relationship between E_R, T_e, and q as obtained from Eq. (30). It is seen that T_e increases with E_R, but decreases with increasing values of q. From Eq. (23) it is evident that measurement of E_R can serve as a substitution for the measurement of P/L.

In Fig. 5 P/L is plotted vs. q with T_e as a parameter. For constant T_e, q increases with P/L, which indicates that the profiles of both n and n_e will tend towards a more rectangular shape as the power input is increased. This tendency is the stronger, the higher T_e.

The P/L (q, T_e (relationship of Fig. 5 has been combined with the $\bar{n}_t$ (q; T_e) relationship of Eq. (32) to eliminate T_e. The resultant $\bar{n}_t$(q; P/L) relationship is plotted in Fig. 6. Each point in this graph represents a solution of the electron balance equation for some particular input conditions P/L; $\bar{n}_t$, and it permits one to read off immediately the appropriate value of q. The curves show that if P/L is low or if $\bar{n}_t \longrightarrow n(Xe)$ ($\approx 6.6 \times 10^{16} cm^{-3}$), $q \longrightarrow 0$, that is, distortion of the profiles is small. $n_e(r)$ then follows the regular Bessel function and n(r) is uniform. Vice versa, as P/L is increased or $\bar{n}_t$ is reduced, the value of q increases.

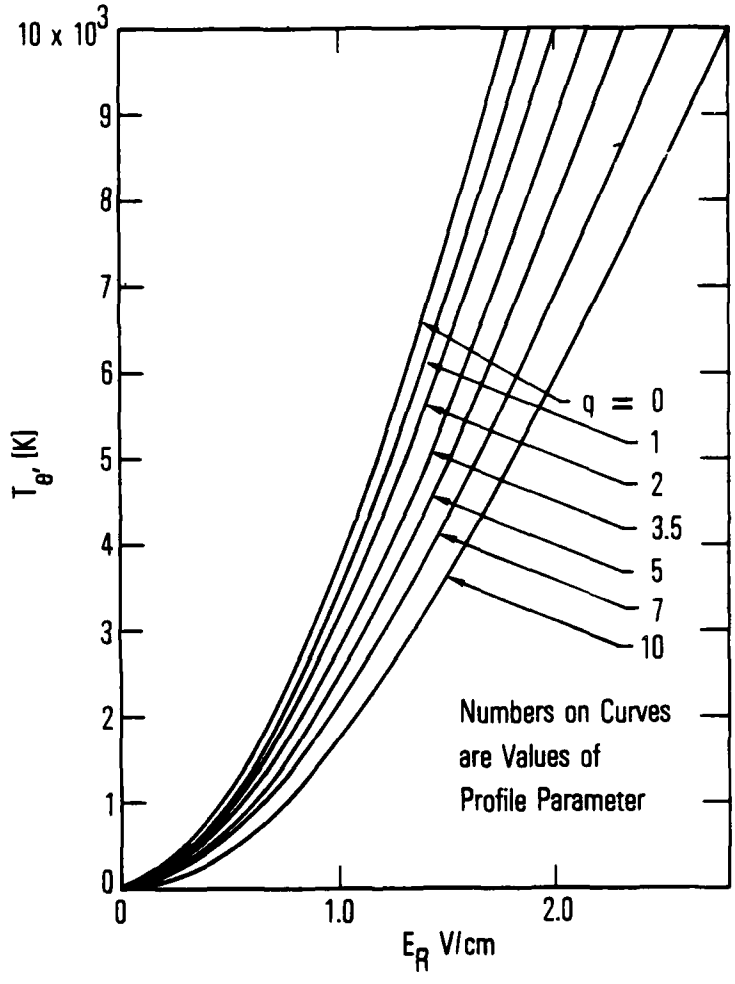

Figure 4. Electron Temperature vs Induced Electric Field at Tube Wall for rf Induction Discharge in Rb-Xe Mixture

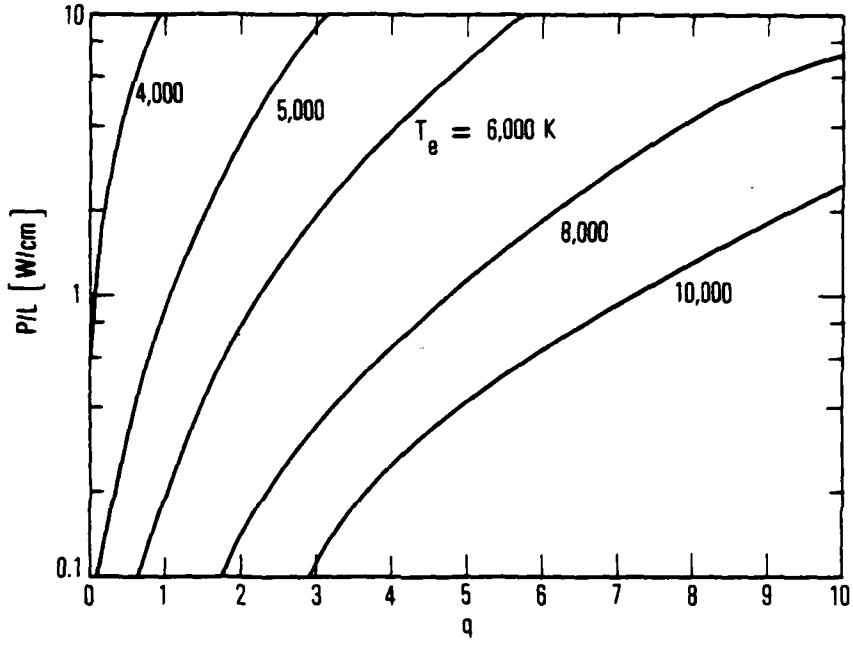

Figure 5. Power Input per Unit Column Length vs Profile Parameter for Various Electron Temperatures in rf Induction-Excited Rb-Xe Discharge

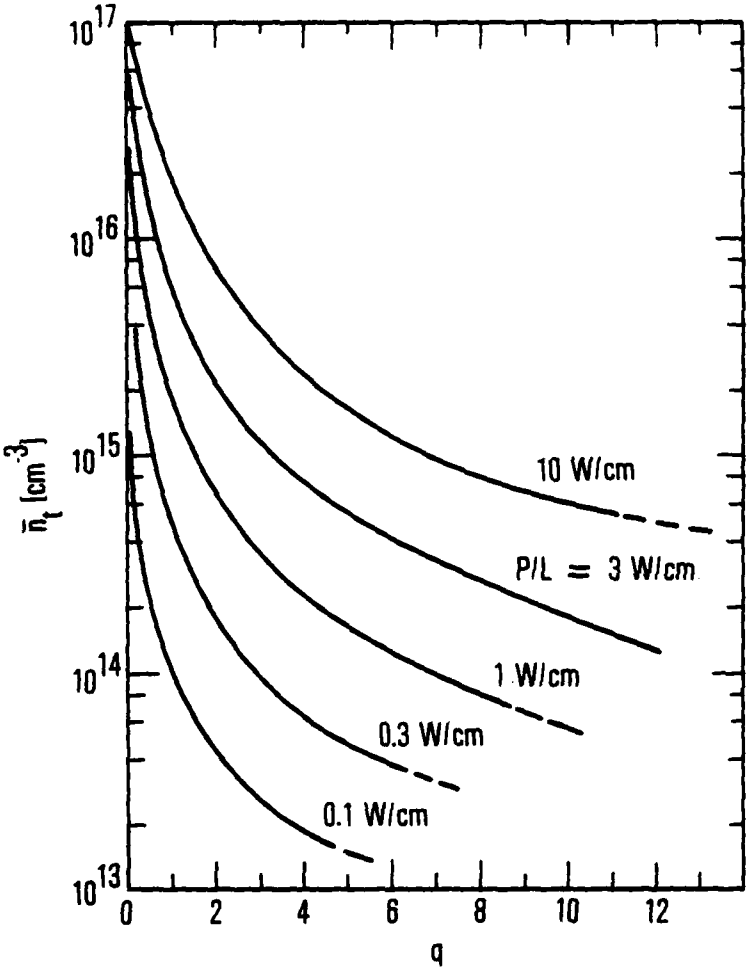

Figure 6. Dependence of Profile Parameter on Mean Total Rb-Particle Concentration for Various Power Inputs per Unit Column Length into rf Induction Discharge in Rb-Xe Mixture

The values of n_R and n_{e_o} have likewise been evaluated as functions of P/L and $\bar{n}_t$ and are plotted in Figs. 7 and 8, respectively. It is seen from Fig. 7 that n_R increases with both $\bar{n}_t$ and P/L. At $\bar{n}_t$ values less than $10^{14}/cm^3$ the increase is approximately proportional to $\bar{n}_t^{1/2}$, as $\bar{n}_t$ becomes larger the exponent increases, and for $\bar{n}_t$ larger than $10^{16}/cm^3$ it is about 1. The effect of P/L on n_R decreases with increasing $\bar{n}_t$. This behavior can be readily understood from the consideration that the transport of Rb-particles to the wall and the buildup of concentration require the expenditure of energy. The higher the energy available per particle, the higher the buildup can go over the average concentration. When comparing n_R with $\bar{n}_t$, it must be remembered that the former refers to atoms only, whereas the latter also comprises ions. Thus even for $n_R = \bar{n}_t$, the concentration of atoms at the wall exceeds their average concentration in the plasma volume. From Fig. 8 it is seen that also n_{e_o} increases with both $\bar{n}_t$ and P/L. The trends here are, however, opposite to those for n_R. The effect of $\bar{n}_t$ is largest at low concentrations and that of P/L is largest at high concentrations of $\bar{n}_t$.

In Fig. 9 the degree of ionization $\alpha \equiv \bar{n}_e/\bar{n}_t$ is shown as a function of $\bar{n}_t$ and P/L. Within the range of parameters considered it can vary between about 1% and 35%. As one would expect, α increases with P/L but decreases with $\bar{n}_t$. The intersection of the curves for P/L = 3 W/cm and 10 W/cm is believed to be real. To the higher P/L value corresponds a higher value of q (Fig. 6) and thus a spreading of the n_e^- distribution closer to the wall where the induced electric field is higher. This causes a higher local power dissipation ($\sim E^2$), so that for the same average ionization one can have different power inputs. If unrestricted, the discharge would operate at the highest input, but in practice this negative characteristic of the discharge is usually compensated by the positive characteristic of the rf power supply which forces stable operation at some intermediate power level.

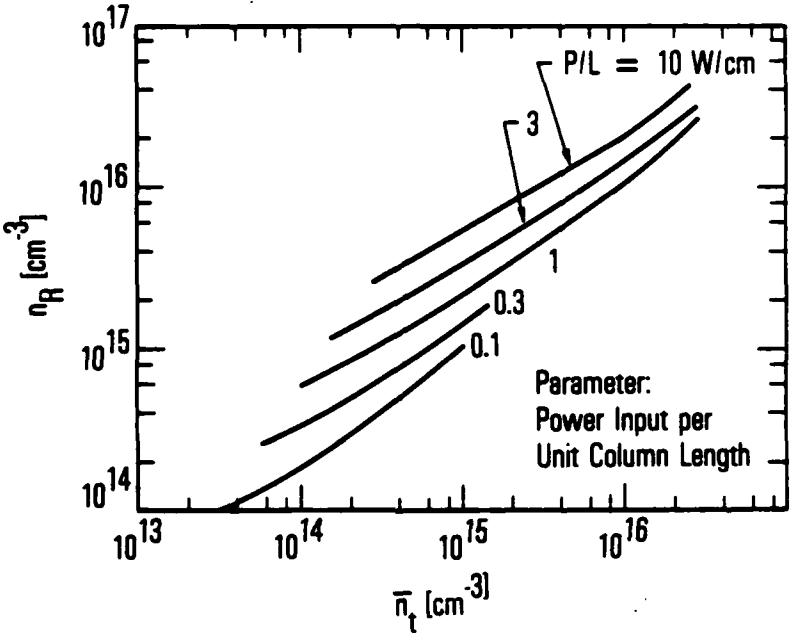

Figure 7. Rb-Atom Concentration at Tube Wall vs Total Mean Rb-Particle Concentration for Inductive rf Discharge in Rb-Xe Mixture

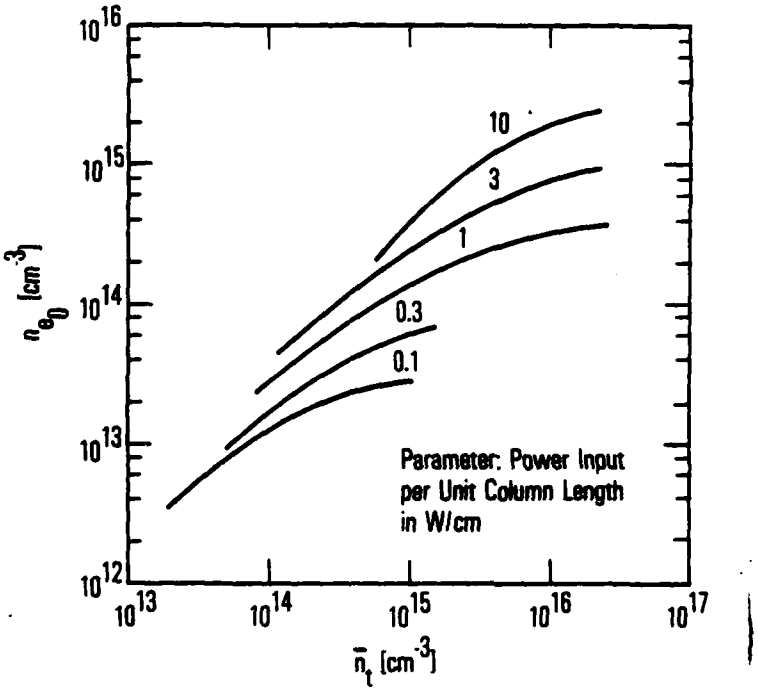

Figure 8. Peak Electron Concentration at Axis vs Mean Total Rb-Particle Concentration for Rb-Xe rf Discharge Column

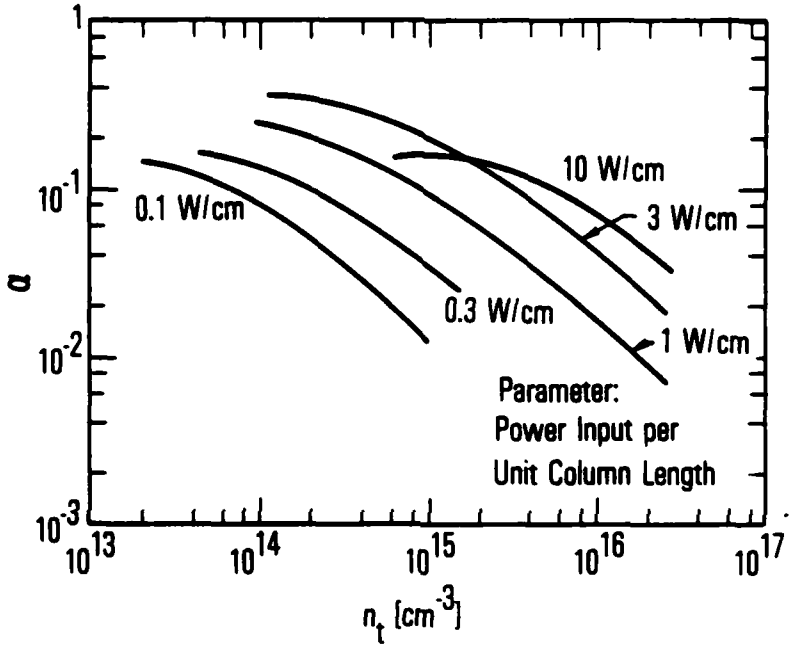

Figure 9. Degree of Ionization of Rb Particles vs Total Mean Rb-Particle Concentration for Inductive rf Discharge in Rb-Xe Mixture

b) Examples for the Radial Distributions of Electrons and Rb Atoms

With the information presented in Figs. 6 - 8 we can now calculate absolute radial distributions of n and n_e from Eqs. (9) and (11) (with (12)) for arbitrary values of $\bar{n}_t$ and P/L and a fixed radius R = 0.4 cm. Such calculations have been carried out for two examples. In the first one $\bar{n}_t = 10^{14} cm^{-3}$ and P/L = 0.3 W/cm were chosen. This yields from the above figures q = 2.5, $n_R = 2.35 \times 10^{14} cm^{-3}$ and $n_{e_o} = 1.70 \times 10^{13} cm^{-3}$. We further obtain from Figs. 5 and 4, $T_e \sim 7500$ K and $E_R \sim 1.75$ V/cm. The corresponding distributions are plotted in Fig. 10. Note the difference in scales between n_e and n. It is seen that n_e is nearly constant over the first 2 mm of the radius and then drops with increasing slope towards the zero value at the wall. The distribution of n shows the inverse behaviour rising from a small fraction, to the wall value in the outer half of the radius.

In the second example P/L has been increased by a factor ten to 3 W/cm for the same $\bar{n}_t = 10^{14}/cm^3$. This yields $q \approx 13$, $n_R = 9 \times 10^{14}/cm^3$, $n_{e_o} = 4 \times 10^{13}/cm^3$, $T_e \sim 10^4$K and $E_R \sim 3$ V/cm. The profiles obtained for these more extreme conditions are shown in Fig. 11. Compared to the first example the regions of uniform distributions of n_e and n have been extended and now encompass 75% of the tube radius, so that practically all Rb atoms are concentrated within one mm from the wall.

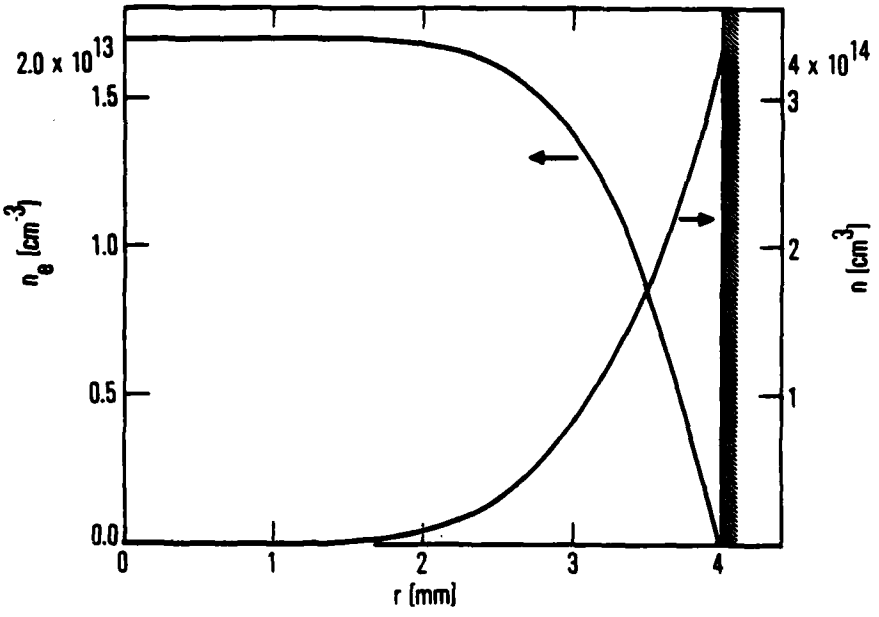

Figure 10. Radial Distributions of Rb-Atom Density n and Electron Density n_e in rf Induction-Excited Rb-Xe Discharge Column P/L = 0.3 W/cm; $\bar{n}_t$ (Rb) = $10^{14}/cm^3$

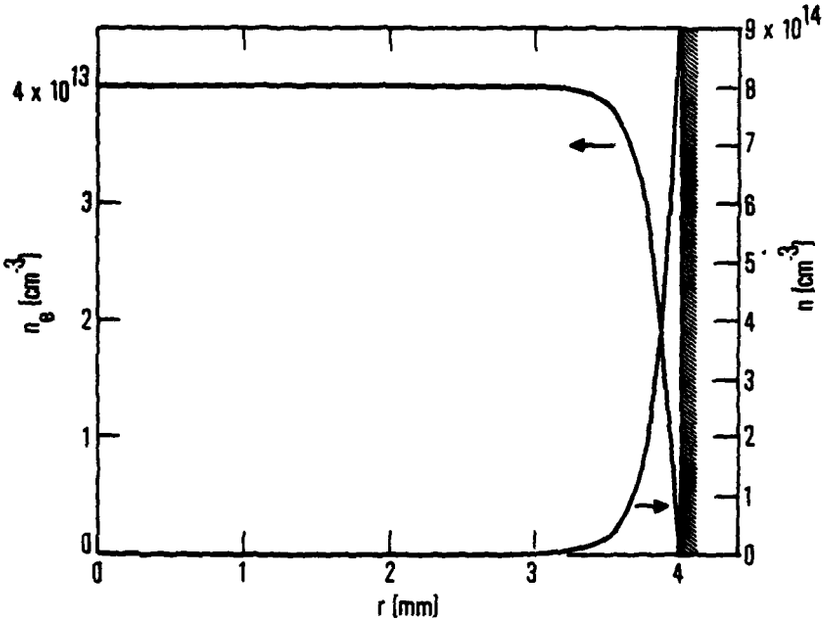

Figure 11. Radial Distributions of Rb-Atom Density n and Electron Density n_e in rf Induction-Excited Rb-Xe Discharge Column P/L = 3 W/cm; $\bar{n}_t$ (Rb) = $10^{14}/cm^3$

V. DISCUSSION

There are at present no experimentally determined particle profiles or related data from induction discharges with which the material of Figs. 6-11 can be compared. The closest data for comparison are the measurements by Dutch workers in the positive column of Cs - Ar dc discharges. The shape of the n_e - profiles obtained by Waszink and Polman [4] is similar to those in Figs. 10 and 11. Also, the Cs-atom density profiles by Bleekrode and v.d. Laarse [3] and by van Tongeren [5, 6] agree, for the higher discharge currents, qualitatively with the Rb profiles in the above figures. The trend towards a more rectangular profile shape with increasing P/L, evident from Figs. 10 and 11, is observed in the above experiments as a function of discharge current.

With respect to Rb discharges in Ne, Ar, or Kr, Tako et al. [18] and Hirano [19] concluded from their observations on spherical lamps that emitting as well as absorbing Rb atoms are concentrated near the walls.

Regarding the electron temperatures, preliminary experiments at The Aerospace Corporation with Rb-Xe induction discharges of the same radius as used in the calculations indicate that the calculated values may be too high by a factor of two or three. Several features in the model may contribute to such a discrepancy. The major cause is probably an underestimation of the electron production rate by disregarding multi-step ionization, especially two-step ionization via the first excited state [7, 8.] Such multiple-step processes become important at higher ionization levels. They require adding terms proportional to n_e^2 and higher powers in n_e to the electron balance equation (52) and thus make this equation nonlinear.

In addition to the underestimation of production rates it is also likely that the model in its present form overestimates electron - Rb ion loss rates. The assumed distribution of Rb atoms according to Eq. (9) involves $n_o = 0$ for all values of $q > 0$, so that there is no electron production at the axis.

This condition will be approached for high values of P/L, but at low inputs we must expect n_o to be nonnegligible. Electrons produced at the axis will have the longest distance to travel to the wall; they will thus in the average have the longest life in the discharge and need to be replaced at a slower rate. Excluding electron production from the central region and shifting it closer to the wall will require higher production rates which are associated with higher values of T_e and/or $\bar{n}_t$.

Allowing for a finite concentration of Rb atoms at the axis according to

$$n = n_o + n_R \rho^{2q} \tag{9a}$$

would make the assumptions in the model more consistent for low P/L and large $\bar{n}_t$. Since the addition of $n_o \neq 0$ would leave the production rates linear in n_e under otherwise unchanged conditions (no consideration of multistep ionization), the solution for the space-dependent term in Eq. (9a), which is Eq. (11), could be superimposed on the solution for the constant term which is the ordinary Bessel function. The resulting increase in complexity of the analysis would be moderate.

The electron temperature does not appear explicitly in the data of Figs. 6 - 11. It will affect them mainly through its influence on D_a (Eq. 43). Having this value too high will, according to Eq. (15), yield too-high levels of $\bar{a}$ relative to $\bar{n}_e$.

Aside from these apparent deficiencies of the present model, it is believed to give a qualitatively correct picture of the conditions in an alkali metal - noble gas discharge and of the relationships involved.

A conclusion that can be drawn from the results with respect to the retention of Rb particles at the wall, mentioned in the introduction, is that lowering the total Rb particle concentration $\bar{n}_t$ (by lowering the vapor pressure) does not cause a proportionate decrease in the wall concentration n_R, since the remaining particles are driven that much harder to the wall.

It is also necessary to reduce the power input P/L to the lowest value consistent with the required emission intensity to minimize Rb losses and enhance the life of the radiation source.

VI. REFERENCES

[1] J.F. Waymouth, Electric Discharge Lamps, the M.I.T. Press, Cambridge, Mass. (1971), p. 194.

[2] M.A. Cayless, "Theory of the Positive Column in Mercury-Rare Gas Discharges," Brit. J. Appl. Phys. 14, pp. 863-869 (1963).

[3] R. Bleekrode and J.W. v.d. Laarse, "Optical Determination of Cs Ground State Depletion in Cs-Ar Low-Pressure Discharges, II. Radial and Axial Cs-Atom Distributions," J. Appl. Phys. 40, pp. 2401-2403 (1969).

[4] J.H. Waszink and J. Polman, "Cesium Depletion in the Positive Column of Cs-Ar Discharges," Appl. Phys. 40, pp. 2403-2408 (1969).

[5] H. van Tongeren, "Radial Density Distribution Measurements of Neutral Cs in the Positive Column of a Cs-Ar dc Discharge," J. Appl. Phys. 42, pp. 3011-3012 (1971).

[6] H. van Tongeren, "Electron Temperature and Radial Density Distribution of Cs Ground State Atoms in the Positive Column of a Cs-Ar dc Low Pressure Discharge," Phys. Letters 37A, pp. 317-318 (1971).

[7] R. Bleekrode and H. van Tongeren, "Measured and Calculated Cs Excited State Densities in Cs-Ar Low-Pressure Discharges," J. Appl. Phys. 44, pp. 1941-1942 (1973).

[8] L. Vriens, "Energy Balance in Low-Pressure Gas Discharges," J. Appl. Phys. 44, pp. 3980-3989 (1973).

[9] H. van Tongeren, "Positive Column of the Cs-Ar Low-Pressure Discharge," J. Appl. Phys. 45, pp. 89-96 (1974).

[10] H. van Tongeren and J. Heuvelmans, "Positive Column of Na-Ar and Na-Ne-Ar dc Low-Pressure Discharges," J. Appl. Phys. 45, pp. 3844-3850 (1974).

[11] L. Vriens, "Two and Three Electron Group Models for Low-Pressure Gas Discharges," J. Appl. Phys. 45, pp. 1191-1195 (1974).

[12] L. Vriens and F.A.S. Ligthard, "Energy Balance and Coulomb Relaxation in Low-Pressure Gas Discharges," Philips Research Reports 32, pp. 1-7 (1977) Netherlands.

[13] W.E. Bell, A.L. Bloom, and J. Lynch, "Alkali Metal Vapor Spectral Lamps," Rev. Sci. Instrum. 32, pp. 688-692 (1961).

[14] V.B. Gerard, "Laboratory Alkali Metal Vapor Lamps for Optical Pumping Experiments," J. Sci. Instrum. 39, pp. 217-218 (1962).

[15] R.G. Brewer, "High Intensity, Low Noise Rubidium Light Source," Rev. Sci. Instrum. 32, pp. 1356-1358 (1961).

[16] R.J. Atkinson, G.D. Chapman, and L. Krause, "Light Sources for the Excitation of Atomic Resonance Fluorescence in Potassium and Rubidium," J. Opt. Soc. Am. 55, pp. 1269-1274 (1965)

[17] H. Oyamada, K. Takahashi, Y. Sato, and H. Uchida, "A Consideration of Rubidium Lamp Stability for Rubidium Frequency Standard," Proc. 28th Annual Sympos. on Frequency Control (1974).

[18] T. Tako, Y. Koga, and I. Hirano, "Spectral Profiles of Rb-D Lines," Japanese J. Appl. Phys. 14, pp. 591-598 (1975).

[19] I. Hirano, "Spectre de la Raye du Rb Dans le Cas d'une Lampe Spherique," Rev. de Phys. Appliquee 12, pp. 1253-1262 (1977).

[20] H.U. Eckert, "Analysis of Thermal Induction Plasmas Dominated by Radial Conduction Losses," J. Appl. Phys. 41, pp. 1520-1528 (1970).

[21] F. Cabannes, "Etude de la Decharge Electrique par Induction dans les Gaz Rares," Ann. de Phys. 12^{e} Ser. 10, pp. 1027-1077 (1955).

[22] K. Eidmann, "Spatial Variation of the Electron Energy in a H.F. Ring Discharge," Zs. f. Physik 238, pp. 189-194 (1970).

[23] D.R. Keefer, "The Theory and the Diagnosis of the Electrodeless Discharge," Ph.D. Thesis, University of Florida (1967), University Microfilms, Ann Arbor, Michigan.

[24] G. Turban, "Etude de la Temperature et de la Densite Electronique d'une Decharge H.F. Inductive dans le Hydrogene, par la Methode de la Sonde Double Symmetrique," Compt. Rend. Acad. Sc. Paris 273, Ser. B, pp. 533-536 (1971).

[25] E.W. McDaniel, Collision Phenomena in Ionized Gases, John Wiley and Sons, Inc., New York, New York (1964).

[26] L. Loeb, Basic Processes of Gaseous Electronics, University of California Press, Berkeley and Los Angeles, California (1960).

[27] J.T. Tate and P.T. Smith, "Ionization Potentials and Probabilities for the Formation of Multiply Charged Ions in the Alkali Vapors and in Krypton and Xenon," Phys. Rev. 46, pp. 773-776 (1934).

[28] G.O. Brink, "Absolute Ionization Cross Sections of the Alkali Metals," Phys. Rev. 134, pp. A345-A346 (1964).

[29] R.H. McFarland and J.D. Kinney, "Absolute Cross Sections of Lithium and Other Alkali Metal Atoms for Ionization by Electrons," Phys. Rev. 137, pp. A1058-A1061 (1965).

[30] A.M. Devyatov, T.N. Solov'ev, and L.M. Volkova, "Study of the Positive Column in the Vapors of Alkali Metals: Effective Cross Sections and Excitation of the Energy Levels," High Temp. (U.S.S.R) 13, pp. 245-249 (1975).

[31] L.M. Volkova, A.M. Devyatov, and T.N. Solov'ev, "Study of the Positive Columns in Alkali Metal Vapors: Population of the Energy Levels," High Temp. (U.S.S.R) 12, pp. 1019-1022 (1974).

[32] T.N. Solov'ev, L.M. Volkova, and A.M. Devyatov, "Positive Column of a Discharge in Alkali Metal Vapor: Effective Cross Sections and Mechanism of Ionization," High Temp. (U.S.S.R) 13, pp. 631-635 (1975).

[33] "Study of the Positive Column of Alkali Metal Vapor Discharges: Probe Measurements," High Temp. (U.S.S.R) 12, pp. 616-619 (1974).

[34] T. Solov'ev, "Energy Balance in Low-Pressure Alkali Metal Vapor Discharges," J. Phys. D: Appl. Phys. (Great Britain) 13, pp. 1291-1297 (1980).

[35] A. von Engel, Ionized Gases, Oxford, Clarendon Press (1965).

[36] H. Margenau, "Conduction and Dispersion of Ionized Gases at High Frequencies," Phys. Rev. 69, pp. 508-513 (1946).

LABORATORY OPERATIONS

The Laboratory Operations of The Aerospace Corporation is conducting experimental and theoretical investigations necessary for the evaluation and application of scientific advances to new military space systems. Versatility and flexibility have been developed to a high degree by the laboratory personnel in dealing with the many problems encountered in the nation's rapidly developing space systems. Expertise in the latest scientific developments is vital to the accomplishment of tasks related to these problems. The laboratories that contribute to this research are:

Aerophysics Laboratory: Launch vehicle and reentry aerodynamics and heat transfer, propulsion chemistry and fluid mechanics, structural mechanics, flight dynamics; high-temperature thermomechanics, gas kinetics and radiation; research in environmental chemistry and contamination; cw and pulsed chemical laser development including chemical kinetics, spectroscopy, optical resonators and beam pointing, atmospheric propagation, laser effects and countermeasures.

Chemistry and Physics Laboratory: Atmospheric chemical reactions, atmospheric optics, light scattering, state-specific chemical reactions and radiation transport in rocket plumes, applied laser spectroscopy, laser chemistry, battery electrochemistry, space vacuum and radiation effects on materials, lubrication and surface phenomena, thermionic emission, photosensitive materials and detectors, atomic frequency standards, and bioenvironmental research and monitoring.

Electronics Research Laboratory: Microelectronics, GaAs low-noise and power devices, semiconductor lasers, electromagnetic and optical propagation phenomena, quantum electronics, laser communications, lidar, and electro-optics; communication sciences, applied electronics, semiconductor crystal and device physics, radiometric imaging; millimeter-wave and microwave technology.

Information Sciences Research Office: Program verification, program translation, performance-sensitive system design, distributed architectures for spaceborne computers, fault-tolerant computer systems, artificial intelligence, and microelectronics applications.

Materials Sciences Laboratory: Development of new materials: metal matrix composites, polymers, and new forms of carbon; component failure analysis and reliability; fracture mechanics and stress corrosion; evaluation of materials in space environment; materials performance in space transportation systems; analysis of systems vulnerability and survivability in enemy-induced environments.

Space Sciences Laboratory: Atmospheric and ionospheric physics, radiation from the atmosphere, density and composition of the upper atmosphere, aurorae and airglow; magnetospheric physics, cosmic rays, generation and propagation of plasma waves in the magnetosphere; solar physics, infrared astronomy; the effects of nuclear explosions, magnetic storms, and solar activity on the earth's atmosphere, ionosphere, and magnetosphere; the effects of optical, electromagnetic, and particulate radiations in space on space systems.

• • •


FILMED
9-8